Hot, dry and windy conditions that drove devastating Pantanal wildfires 40% more intense due to climate change

Authors

1. Clair Barnes, *Grantham Institute, Imperial College London, UK*
2. Filippe LM Santos, *Instituto de Ciências da Terra, Instituto de Investigação e Formação Avançada, Universidade de Évora, Portugal & Instituto de Geociências, Universidade Federal do Rio de Janeiro, Brasil*
3. Renata Libonati, *Instituto de Geociências, Universidade Federal do Rio de Janeiro, Brasil*
4. Theo Keeping, *School of Archaeology, Geography and Environmental Science, University of Reading & Leverhulme Centre for Wildfires, Environment and Society, Imperial College London*
5. Regina Rodrigues, *Univ. Federal de Santa Catarina, Florianópolis, Brazil*
6. Lincoln Muniz Alves*, Instituto Nacional de Pesquisas Espaciais (INPE), São Paulo, Brazil*
7. Sajanika Sivanu, *Red Cross Red Crescent Climate Centre, the Hague, the Netherlands (based in Toronto, Canada)*
8. Maja Vahlberg, *Red Cross Red Crescent Climate Centre, the Hague, the Netherlands (based in Ubmeje/Umeå, Sweden)*
9. Tilly Alcayna, *Red Cross Red Crescent Climate Centre, the Hague, the Netherlands (based in London, the UK)*
10. Fredi Otto, *Grantham Institute, Imperial College London, UK*

Review authors

1. Mariam Zachariah, *Grantham Institute, Imperial College London, UK*
1. Roop Singh, *Red Cross Red Crescent Climate Centre, the Hague, the Netherlands (based in New Jersey, USA)*
2. Miqueias Mugge, *Brazil LAB, Princeton University, Princeton, USA*
3. João Biehl, *Brazil LAB, Princeton University, Princeton, USA*
4. Adriana Petryna, *University of Pennsylvania, Philadelphia, USA*
5. Mariana Dias, *MapBiomas, São Paulo, Brazil*
6. Eduardo Reis, *MapBiomas, São Paulo, Brazil*
7. Sara Uzquiano, *European Forest Institute, Bonn, Germany*

Main findings

- Fire weather is a critical driver of wildfires, although changes in vegetation (wildfire fuel) and fire management strategies also contribute to future wildfire risk. In the Pantanal, land use and land cover changes, such as clearing natural vegetation for pasture or agriculture, contribute to drier conditions and increase the availability of flammable vegetation.

- In today's climate with 1.2°C of global warming, intense fire weather conditions like the ones that drove the wildfires in the Brazilian Pantanal during June 2024 are a relatively rare event, expected to occur once every 35 years. This means there is about a 3% chance similar June fire weather conditions will occur in any given year.
- Observations show that similar June fire weather conditions, as defined by DSR, are about 3 times more impactful than they would have been in a 1.2°C cooler climate. They would have been about a factor 100 rarer had the climate not been warmed by humans.
- To determine the role of climate change, we combine fire weather observations with climate models. Human-induced warming from burning fossil fuels made the June 2024 DSR about 40% more impactful and 4-5 times more likely.
- These trends will continue with future warming. If warming reaches 2°C, similar June fire weather conditions will become around twice as likely, expected to occur on average about once every 17 years, and will become 17% more impactful.
- To understand how the June fire-weather conditions are affected by human-induced climate change, we also investigate the weather variables comprising the DSR: maximum temperature, relative humidity, wind speed and rainfall. Most of these variables broke records in June 2024: it was the driest, hottest, and windiest June since observations began. Only relative humidity was the second lowest on record.
- Next, we analyse how climate change alters likelihood and intensity of these four main weather variables. In the observations there is a strong drying trend and, as expected, increasingly high temperatures (figure 1b) accompanied by a reduction in relative humidity, while there is no clear trend in wind speeds. Thus, the increase in DSR can be explained by increasing temperatures - driven by climate change - and decreasing rainfall.
- Yearly rainfall in the Pantanal has been decreasing for over forty years. While natural decadal variability and deforestation in large ecosystems are known to affect rainfall patterns across South America, climate change may also be influencing the drying trend.
- The June 2024 fires spawned multi-ministry response actions to try to contain fires and save wildlife and livelihoods, such as the establishment of 13 new bases to accelerate the deployment of firefighters to remote areas. However, while significant steps have been taken to address the Pantanal wildfires, there are still substantial challenges to containment and extinguishment efforts. It is imperative that government agencies at all levels act swiftly and prepare for increasingly critical situations, as projections indicate a rise in such events.

1 Introduction

During June 2024, the Pantanal wetlands experienced record numbers of wildfires for the time of year (Figure 1). The fire season in the Pantanal usually starts in July and peaks between August and October (Libonati et al., 2022a; Silva et al., 2024); fires are usually the result of human activity, with atmospheric discharges (lightning) responsible for only 1% of fire events (Menezes et al., 2022). This year's exceptionally hot and dry weather has produced tinderbox conditions much earlier in the year that have enabled fires to spread out of control (Libonati et al., 2024). As a result, more than 400,000ha have burned (ALARMES), much of it in the provinces of Mato Grosso and Mato Grosso do Sul in Brazil around the Paraguay river (Figure 1.2, left panel). Moreover, reports from media indicated that people, notably children and the elderly, experienced respiratory issues as a result of the particulate pollution from fire smoke and hospitals were overcrowded (Guardian, 2024). In the

municipality of Corumbá, health centres and hospitals are reported to be crowded with individuals experiencing respiratory issues (Barber, 2024). Wind can carry particulate pollution long distances and ash fall can pollute rivers, deteriorating water quality and affecting people's safe access to water (FioCruz, 2024; Dos Santos et al., 2024).

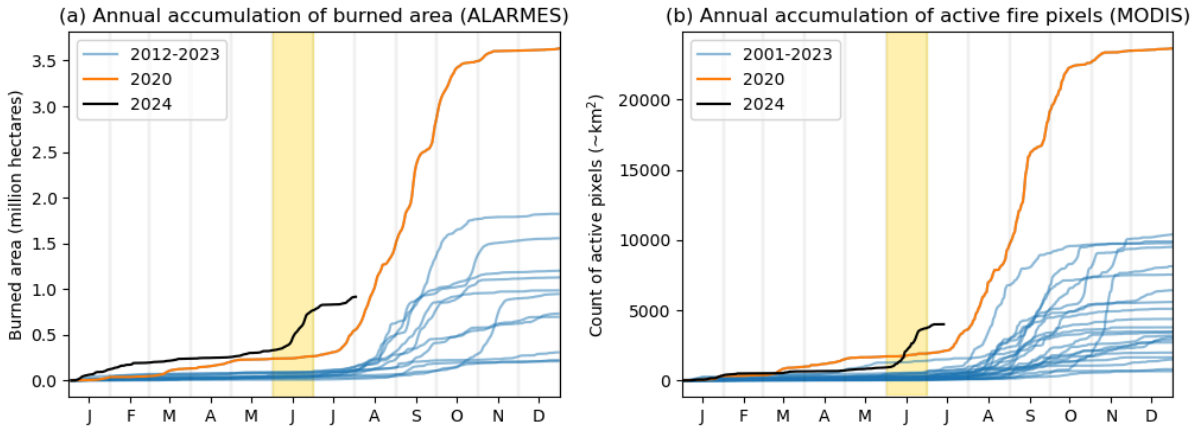

***Figure 1.1**: **(right)** accumulated* burned area in Pantanal based on ALARMES product (2012-2024); ***(left)** accumulated count of active fire pixels with confidence > 80% within the Brazilian Pantanal, used as a proxy for active fire area (MODIS) (2001-2024)*.

The Pantanal has been experiencing drought conditions since 2018 (Geirinhas et al., 2023), with the Paraguay River reaching historically low levels in April 2024 and critical water scarcity declared in the basin in May (Globo, 2024). With river levels at historic lows, combined with precipitation below the climatological normal, the floods that usually dominate the Pantanal landscape during the austral summer months and extend until autumn (November-April) (Jean Milien, et al., 2023) did not occur this year, making vegetation that would usually be underwater available as a potential fuel source. The regions most affected by the fires predominantly correspond to those with a higher fuel load available for combustion (Figure 1.2, right panel).

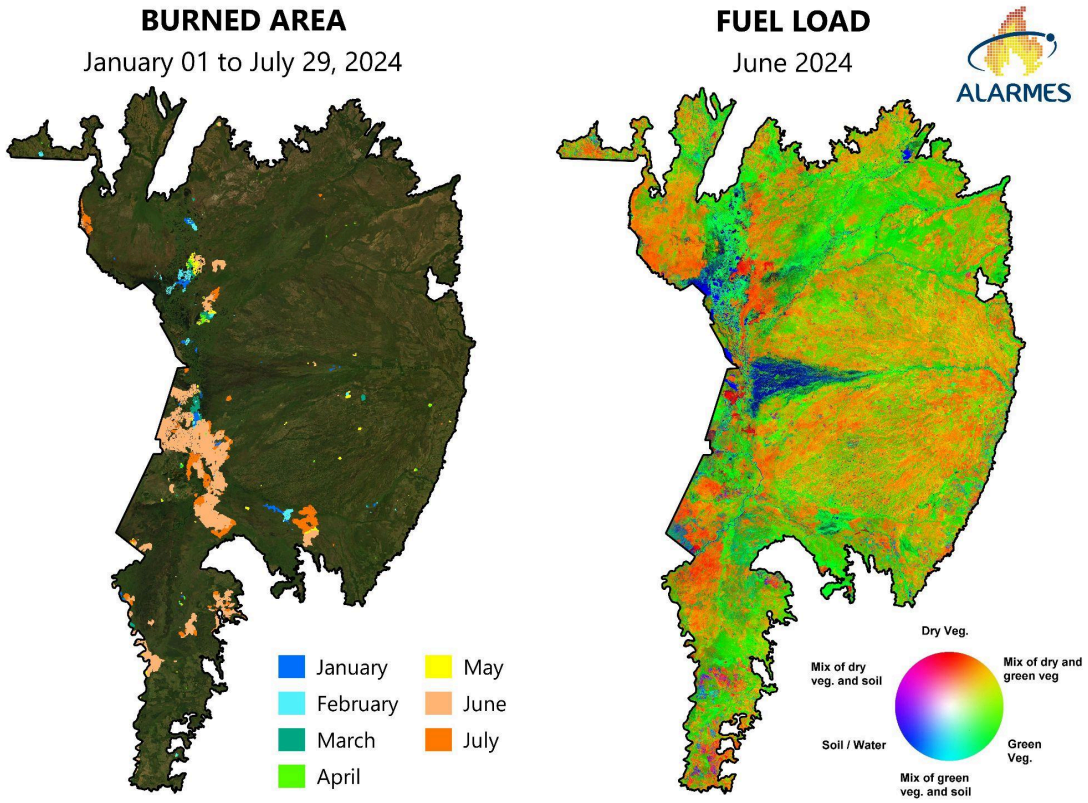

Figure 1.2: *(left) monthly burned area in 2024 and (right) fuel load during June 2024 in the Brazilian Pantanal. Maps provided by* ALARMES.

1.1 Fires in the Brazilian Pantanal

The Pantanal is characterised by a strong seasonal flooding pulse with a wet summer and a dry winter (Alho and Silva, 2012), which contributes to high fuel availability and its natural cycle of fire 'seasons' (Garcia et al., 2021). However, shifts in climate and landscape during the last decades have increased the aridity and significantly aggravated drought and hot conditions (Libonati et al., 2022a; Libonati et al., 2022b; Kumar et al., 2022; Wantzen et al., 2024) and ignition patterns (Menezes et al., 2022; Garcia et al., 2021), leading to a change in the frequency, duration, and severity of fire seasons (Libonati et al, 2022a; Libonati et al., 2022b). In particular, heat wave frequency and extent explain 82% of the interannual variability of burned area in the Pantanal (Silva et al., 2022). Alongside the observed drying trend, the region shows a pronounced warming trend of 0.76°C per decade, responsible for warming of around 3°C since 1980, which has increased the extent and frequency of heatwaves and thus the fire risk (Libonati et al., 2022a).

From 2019 to 2021, the Pantanal experienced recurrent severe fire seasons, with 7 million hectares burned (50% of its area (ALARMES, 2024). The year 2020 was, by far, the worst ever seen: 3.6 million hectares (⅓ of Pantanal area) were burned (Libonati et al., 2020,) with catastrophical ecological and social-economic impacts (Tomas et al., 2022; Silva et al., 2024; Correa et al., 2022; Martins et al., 2022; Santos Ferreira et al, 2023). Compound drought and heat wave (CDHW) conditions played a crucial role during the 2020 fire season: although representing only 37% of the total fire season days, CDHW days accounted for 71% of the total burned area (Libonati et al, 2022a).

A significant increasing trend in heatwave occurrence over Pantanal is projected, which is likely to contribute to drier conditions and more fires during the dry season (Silva et al., 2022).

1.2 Rainfall and flooding in the Pantanal

The Pantanal's seasonality is linked to the South American monsoon system. Its wet season is during austral summer, mainly from December to February, associated with the establishment of the South Atlantic Convergence Zone (SACZ). The SACZ is a band of strong precipitation oriented northwest-southeast associated with a cyclonic (clockwise) circulation that channels moisture from the Amazon towards the Pantanal and southeast Brazil (Carvalho et al., 2002). During the dry season, an anticyclonic (anticlockwise) circulation established over central Brazil can suppress the formation of the SACZ and its related rainfall (Rodrigues & Woollings, 2017). Suppression of the SACZ during the wet season can lead to intense droughts over the Pantanal region during the dry season, as the Pantanal works as a large reservoir, with a lag of up to 5 months between the inflow and outflow (Marengo et al., 2021; Geirinhas et al., 2023). Prolonged periods of drought tend to decrease the river depth, reducing the extent of the floodplains.

Earlier studies have shown that the SACZ varies strongly on intraseasonal time scales, and for this reason, the Madden–Julian oscillation (MJO; Madden and Julian 1994) can modulate the SACZ (Rodrigues & Woollings, 2017; Carvalho et al., 2004). The MJO influences the phase of the midlatitude synoptic disturbances that affect the SACZ (Liebmann et al., 2004). The representation of the MJO in climate models has generally remained unsatisfactory (Jiang et al., 2020), which partially explains the discrepancies between models and observations of the rainfall over the Pantanal. Moreover, other modes of climate variability, such as ENSO, can modulate the MJO-SACZ relationship, making it even more difficult for climate models to simulate the rainfall over the Pantanal (Marengo et al., 2021; Gomes et al., 2021). As a result, historical trends in precipitation over central South America might not be well represented by climate models (Ortega et al., 2021; Gomes et al., 2021). Projected trends in rainfall over South America are mixed due to the complex mechanisms driving precipitation in the area, but studies have found an increase in both the number of consecutive dry days, soil moisture drought and hydrological deficit in the South American Monsoon region (IPCC WG1, ch. 11.6.5). There is also some evidence from future climate model projections that while wet extreme events will become more frequent in the highlands, severe and prolonged droughts will be more prominent in the Pantanal (Thielen et al., 2020; Gomes et al., 2021).

1.3 Event Definition

Monthly severity rating during June

Wildfires in the Pantanal are complex phenomena that are not driven solely by the weather, but also by vegetation properties, land-cover and human activity (Libonati et al., 2022; Libonati et al., 2020). Thus, quantifying the effect of climate change on realised wildfires - for example, on the observed burned area or number of fires - is very difficult (Lui et al., 2022). As such, we only attribute trends in fire-weather conditions, not in wildfire activity.

To reflect the extent and duration of the extreme fire weather across the region, we will use the cumulative daily severity rating (DSR) for the month of June, averaged over the Brazilian Pantanal (solid black outline in Figure 1.3a). We focus on the Brazilian Pantanal rather than the full region, which extends into Bolivia and Paraguay because almost all of the active fires during June 2024 were within the Brazilian part of the biome; however, we would not expect to obtain a different result if we considered the wider region. The DSR reflects how difficult a fire is to suppress once ignition has occurred; it is commonly used for assessing fire weather on monthly or longer timescales (Van Wagner, C. E., 1987). Figure 1.3b shows the relationship between the monthly accumulated DSR (from the ERA5 dataset) and the count of active fire pixels within the Brazilian Pantanal (based on pixels with confidence > 80% in the MODIS dataset, which closely approximates the burned area, as shown in Figure 1.1) between 2001 and 2024. In June the DSR is highly correlated with the log of the active fire area, suggesting that this is a relevant index in this region; even excluding the 2024 event, the correlation is 0.57.

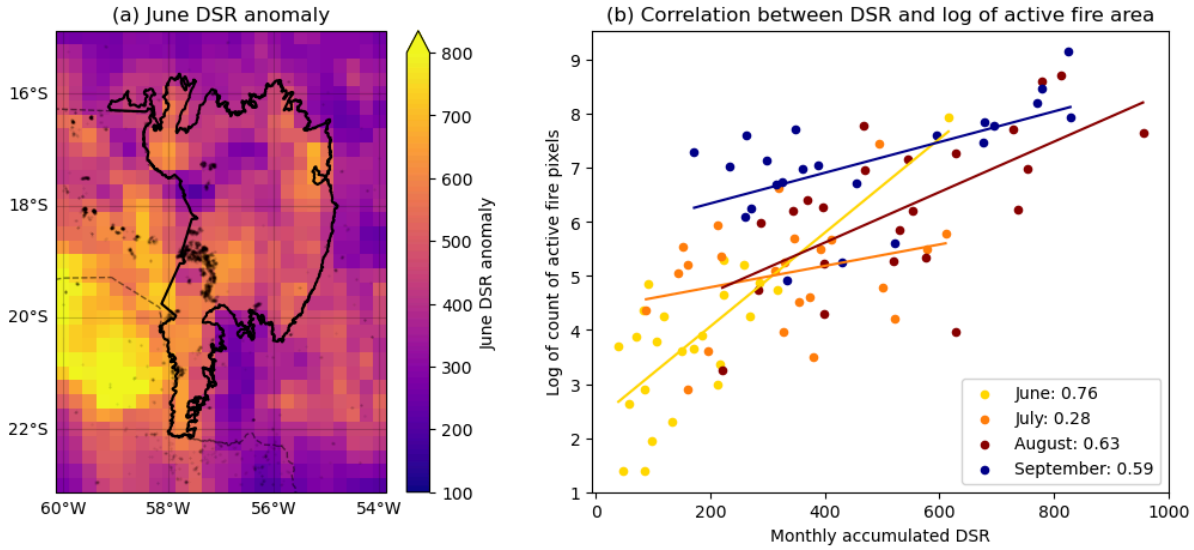

***Figure 1.3**: (a) Map of June 2024 DSR anomaly over the study region wrt 1990-2020 June climatology (ERA5), showing active fire pixels as black dots; (b) correlation between monthly DSR and count of active fire pixels, with correlation coefficient for each month given in brackets. Active fire pixels are pixels with confidence > 80% in MODIS dataset from 2001-2024, used as a proxy for active fire area.*

Annual accumulated precipitation

As Figure 1.4a shows, the region has become progressively warmer and drier in recent decades. Figure 1.4b shows the annual precipitation anomaly from July 2023-June 2024, relative to the annual climatology from 1990-2020. The whole of the Pantanal was in drought at this time, receiving just 56% of the 1990-2020 mean annual rainfall. To examine the likely role of climate change in enhancing these drought conditions, which have contributed to the high DSR and so to the high level of fire activity in June 2024, we evaluate trends in annual (July-June) precipitation over the same region (black outline in Figure 1.4b).

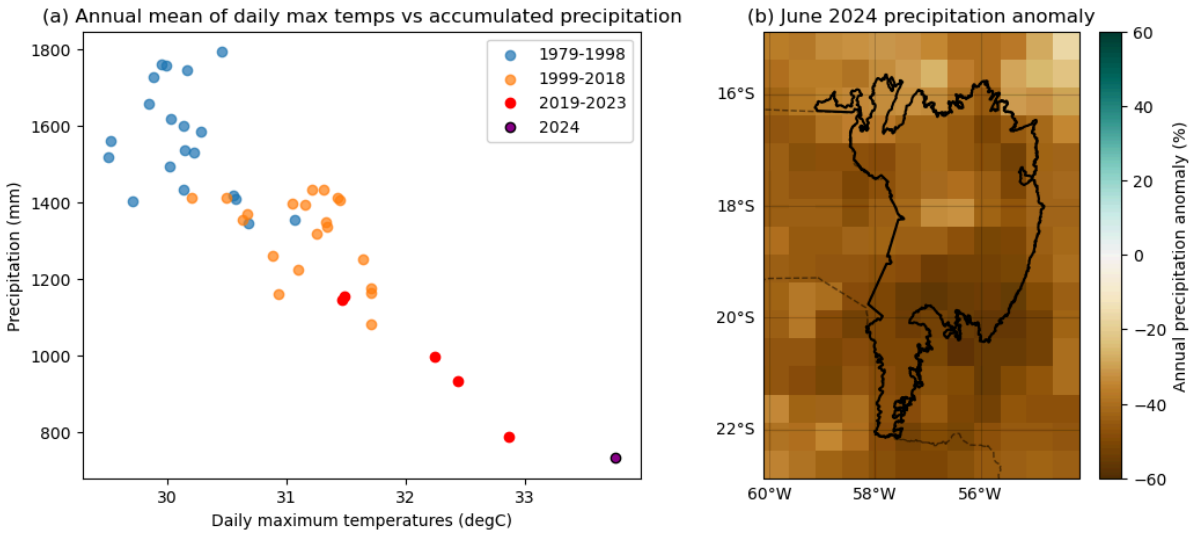

***Figure 1.4**: (a) July-June annual mean of daily maximum temperatures and accumulated precipitation over the Brazilian Pantanal since the beginning of the satellite era; (b) map of annual precipitation anomaly, relative to 1990-2020 climatology (both using ERA5).*

2 Data and methods

2.1 Calculation of the Fire Weather Index and Daily Severity Rating

In this study, the accumulated daily severity rating (DSR) is used to quantify the likely risk of extreme wildfires due to the prevailing weather conditions. The DSR is derived from the Fire Weather Index (FWI), which uses meteorological information to predict the expected energy release per length of the fire-front if a wildfire occurs (Van Wagner, 1974), and is currently used to issue fire weather danger forecasts for the Upper Paraguay basin by ALARMES platform (Nunes et al., 2023). The DSR is a power transformation of the FWI that puts more weight on high values of the FWI, which lead to more rapid spread and fire intensity, and corresponds better to the overall impact of wildfires on the landscape and the consequent effort of suppressing those fires. The DSR can thus be averaged over time and space, to define a cumulative index for wildfire impact over an ecologically similar area (Van Wagner, 1970) and is highly correlated with active fire area in this region (Figure 1.4a).

The Fire Weather Index (FWI) consists of three initial subindices that are calculated using temperature, relative humidity and wind speed at 10m recorded at noon, as well as 24-h precipitation. These subindices are the fine fuel moisture code (FFMC), duff moisture code (DMC) and drought code (DC), with values from the previous day feeding back into the system to model long-term changes in fuel moisture. As shown in Figure 2.1, these three subindices plus windspeed are combined via the initial spread index (ISI) and the buildup index (BUI) to generate the final FWI value.

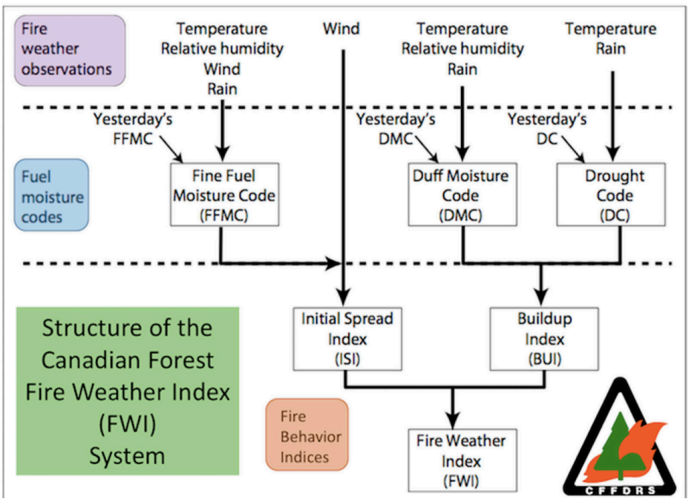

Figure 2.1: *Structure of the Canadian Forest Fire Weather Index (Van Wagner, C.E (1974); image courtesy of UQAM)*

Except for ERA5 and MERRA2 (details below) the FWI was calculated from daily maximum temperatures, accumulated precipitation, mean relative humidity and mean wind speed using the xclim Python package. $DSR = 0.0272\ FWI^{1.77}$ was calculated at each grid cell before averaging over the study region.

2.2 Observational data

Gridded weather data

1. The ERA5 reanalysis product (Hersbach et al., 2020) produced by the European Centre for Medium-Range Weather Forecasts. This product covers the globe at 0.25° resolution, starting in 1950. The variables from ERA5 are not directly assimilated, but are generated by atmospheric components of the Integrated Forecast System (IFS) modelling system. The daily FWI and sub-indices were downloaded directly from Copernicus' Climate Data Store (CDS) at 0.25° resolution; daily maximum temperatures, total precipitation and mean wind speed were downloaded at 0.5° resolution (aggregated from 0.25°) from KNMI's Climate Explorer tool; hourly relative humidity was downloaded from the CDS and averaged in post-processing.

2. MSWX (Multi-Source Weather) dataset (Beck et al., 2022), which combines various observational and reanalysis-based data for reliable bias-corrected weather variable estimates, at 3-hourly intervals from 1979 to near real-time, and at 0.1° spatial resolution globally.

3. The FWI and associated sub-indices computed from the bias-corrected MERRA2 reanalysis product (Gelaro et al., 2017; Reichle et al., 2017) were downloaded from NASA's Global Fire Weather Database (GFWED). This product provides daily data at 0.5° by 0.6° spatial resolution, from 58S to 75N.

4. CHIRPS (Climate Hazards Group InfraRed Precipitation with Station data; Funk et al., 2015b), a daily precipitation-only dataset developed by the UC Santa Barbara Climate Hazards Group, incorporating satellite data, infrared Cold Cloud Duration (CCD) estimates and blended station data. Daily data are available from 1981-present at 0.05° resolution from 60S to 60N.

5. The MERGE product (Rozante et al., 2010, Rozante et al., 2020), available from INPE, combines observed precipitation with satellite precipitation estimates over South and Central America. Daily data are available from 2000-present at 0.1° resolution from 60S to 32.3N and from 120W to 20W.

Active fire area & burned area data

The active fire pixel information shown in Figures 1.2 and 1.3 is taken from NASA's Fire Information for Resource Management System (FIRMS) Moderate Resolution Imaging Spectroradiometer (MODIS MCD14DL) Collection 6. MODIS uses a contextual algorithm (Giglio et al., 2003; Giglio et al., 2016) to detect active fires. Each pixel is classified according to the type of fire detected, along with an associated confidence level, based on the presence or absence of the mid-infrared radiation information typically emitted from fires. Pixels are $1km^2$, therefore this is approximately the minimum size of the fires detectable by MODIS. To minimise the risk of false positive detections, only fire pixels assigned a confidence above 80% are retained.

The burned area data in Figures 1.1 and 1.2 are taken from the ALARMES System, which combines satellite images, active fire information and deep learning to identify the location and extent of burned areas each day in near-real-time. The platform was developed by LASA/UFRJ in partnership with IDL/ULisboa and is currently used by environmental agencies for planning and carrying out effective actions.

Large-scale climate indices

As a proxy for anthropogenic climate change, we use the (low-pass filtered) global mean surface temperature (GMST) taken from the National Aeronautics and Space Administration (NASA) Goddard Institute for Space Science (GISS) surface temperature analysis (GISTEMP, Hansen et al., 2010 and Lenssen et al., 2019).

2.3 Model and experiment descriptions

1. High-resolution regional climate model data were obtained from the Coordinated Regional Climate Downscaling Experiment (CORDEX) multi-model ensemble (Giorgi and Gutowski, 2015; Giorgi et al., 2021). For the South America domain, the ensemble consists of 6 simulations resulting from pairings of 3 Global Climate Models (GCMs) and 2 Regional Climate Models (RCMs) at 0.22° resolution (SAM-22) and 15 simulations resulting from pairings of 10 GCMs and 4 RCMs at 0.44° resolution (SAM-44). These simulations are

driven by historical forcings up to 2005, and extended to the year 2100 using the RCP8.5 scenario.

2. We use 11 simulations from the CMIP6 ensemble (Eyring et al., 2016). For all simulations, the period 1850 to 2015 is based on historical simulations, while the SSP5-8.5 scenario is used for the remainder of the 21st century.

2.4 Statistical methods

Methods for observational and model analysis and for model evaluation and synthesis are used according to the World Weather Attribution Protocol, described in Philip et al., (2020), with supporting details found in van Oldenborgh et al., (2021), Ciavarella et al., (2021) and here. The key steps, presented in sections 3-6, are: (3) trend estimation from observations; (4) model validation; (5) multi-method multi-model attribution; and (6) synthesis of the attribution statement.

In this report we analyse time series of June accumulated DSR and total annual rainfall from July-June, averaged over the Brazilian Pantanal (outlined in solid black in Figure 1.3).

We use a nonstationary normal distribution that shifts linearly with GMST to model log(DSR); this means that the DSR scales exponentially with GMST, so results are presented as % changes in DSR. For precipitation we use a normal distribution that scales exponentially with GMST, with the dispersion (the ratio between the standard deviation and the mean) remaining constant over time. While the normal distribution is unbounded on the real line, and therefore could in theory predict negative precipitation values in the lower tail, in practice the mean of the distribution was far enough from zero that this was not the case, and the distribution was found to be a good fit to the data (see eg. Figure 3.9). The parameters of the statistical models are estimated using maximum likelihood.

For each time series we calculate the return periods, probability ratio (PR; the factor-change in the event's probability) and change in intensity of the event under study for the 2024 GMST and for 1.2C cooler GMST: this allows us to compare the climate of now and of the preindustrial past (1850-1900, based on the Global Warming Index).

3 Observational analysis: return period and trend

3.1 June accumulated DSR

Figure 3.1 shows the time series of log-transformed June cumulative DSR (hereafter log(DSR)) in the ERA5, MSWX and MERRA2 datasets (the corresponding plots for DSR can be found in Figure A1.1 in the Appendix). Where they overlap, all three datasets are highly correlated; while MSWX is derived from ERA5 and so the two are expected to be similar, MERRA2 is independently derived from bias-corrected data, so this similarity suggests a robust trend. In ERA5 and MSWX the event has a return period of 32 and 38 years, respectively (Table 3.1); MERRA2 data for June 2024 were not

available at the time of writing. We therefore use a return period of 35 years to characterise the event for the attribution analysis.

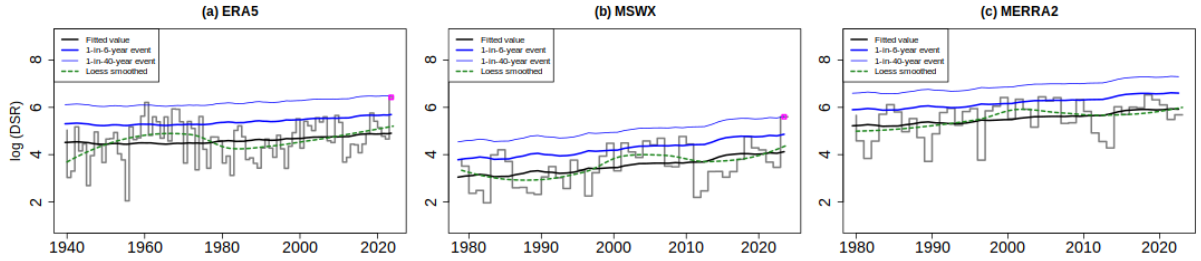

Figure 3.1: *Time series of June log(DSR) averaged over the study region in three observational datasets: ERA5, MSWX and MERRA2. The heavy black line indicates the mean of the nonstationary distribution fitted to the full time series, with the 6-year and 40-year effective return levels in each year in blue. The dashed green line is a nonparametric Loess smoother; the pink dot marks the 2024 total. At the time of writing, data for June 2024 were not yet available for MERRA2 so the event is not shown.*

Table 3.1: *Estimated return period of the 2024 June accumulated DSR, relative change in June accumulated DSR, and change in likelihood of exceeding the observed June accumulated DSR between the 2024 climate and a 1.2ºC cooler climate, in the three observational datasets used in the study. For MERRA2 the change in DSR and probability ratio were estimated for a 1-in-35-year event.*

	ERA5	**MSWX**	**MERRA2**
Return period	31.9	38	-
% change in DSR	65.1 (-11.0, 203)	366 (69.2, 1309)	207 (33.3, 637)
Probability ratio	4.72 (0.67, 32.4)	699 (10.7, 498505)	122 (3.6, 20660)

The fitted trend in log(DSR) in each observational dataset is shown in Figure 3.2. In all cases the linear trend is close to the nonparametrically smoothed trend (dashed green line), although there seems to be a small slowly-varying oscillation not accounted for by the model. In ERA5 the trend is not statistically significant, although the best estimate is an increase of 65% in DSR between a 1.2°C cooler climate and the present; in the shorter MSWX and MERRA2 time series, the estimated trend is stronger and statistically significant, but with much higher uncertainty (Table 3.1).

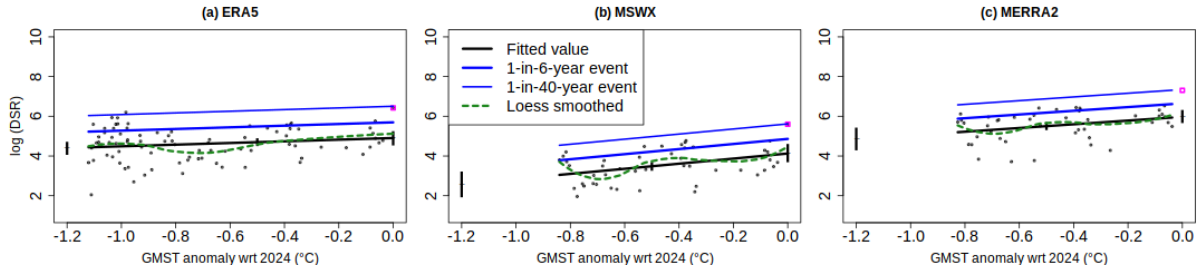

Figure 3.2: *Linear trend in June log(DSR) in ERA5, MSWX and MERRA2 as a function of GMST. The thick black line denotes the mean of the fitted distribution, and the blue lines show estimated 6- and 40-year return levels. The dashed green line is a nonparametric Loess smoother. The vertical lines show the 95% confidence interval for the location parameter for the 2024 climate, 0.5ºC cooler 2000 climate and a hypothetical 1.2ºC cooler climate. The 2024 observation is highlighted in magenta; for MERRA2, this point shows an event with a return period of 35 years in the 2024 climate.*

Figure 3.3 shows the modelled change in return levels of the observed event due to a 1.2°C change in GMST from the preindustrial to the current climate. The points representing the logDSR in ERA5 and MSWX lie within the shaded region indicating the 95% confidence interval, indicating that the chosen statistical model fits the data well, although in MERRA2 the highest DSR values systematically diverge from the expected values; this is reflected in very high uncertainty about the probability ratio and change in DSR. In ERA5 the best estimate of the probability ratio (which is not statistically significant) is 4.8; in MSWX and MERRA2 the event is estimated to be, respectively, 699 times and 122 times more likely due to climate change (Table 3.1).

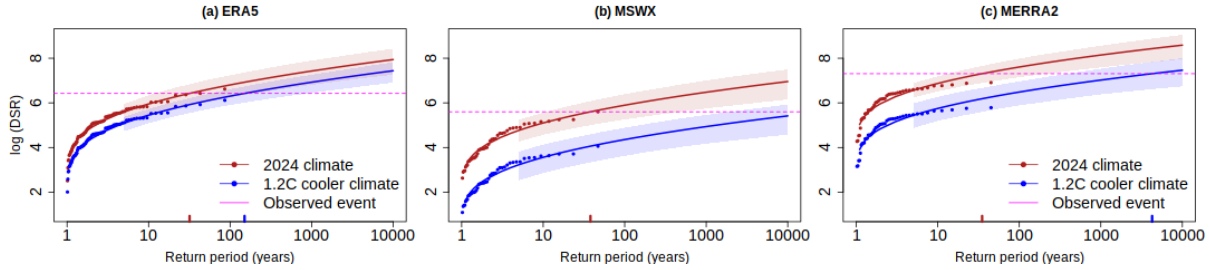

Figure 3.3: *Return levels for June logDSR over the study region at the 2024 GMST (red lines) and 1.2°C lower GMST (blue line), estimated from the statistical model. Shaded regions represent 95% confidence intervals obtained via a bootstrapping procedure. The pink line shows the logDSR during 2024. Red and blue ticks at the x axis indicate the estimated return level of June 2024 in the 2024 climate and 1.2°C cooler climate respectively.*

Overall there is strong evidence in the observations of an increase in June DSR in the last 50 years, albeit with high uncertainty about the strength of the trend; the signal is less clear in ERA5 before 1980, although whether this is due to natural variability or simply less reliable reanalysis prior to the satellite era is not known.

3.1.1 Trends in subindices

In order to understand the likely factors driving the observed increase in fire weather discussed in section 3.1, we now consider trends in the subindices and weather variables that contribute to the fire weather index and hence to the DSR, although no formal attribution is carried out.

Figure 3.4 shows the annual distribution of the DSR and sub-indices in ERA5 averaged over the Brazilian Pantanal, with historical years shown in light blue and 2024 in black and the 95th percentile of the 15-day smoothed 1990-2020 climatology in dark blue; Figure 3.5 shows key weather variables in the same format. From panel (3.4a) we see that the DSR was far above the expected level in the middle of June, reaching levels more usually seen in August. The peaks in DSR closely follow the shape of the initial spread index (ISI, panel 3.4b), which reflects the expected rate of fire spread once ignition has occurred. The ISI depends on the wind speed and the fine fuel moisture code (FFMC), which indicates the expected flammability of fine fuel and typically reflects dry conditions on the scale of a few days; the FFMC was close to its seasonal maximum throughout much of May and June (panel 3.4c) after several weeks of high temperatures and low rainfall (3.5d, a), while the daily wind speeds (3.5c) were above the 95th percentile for much of the month.

The build up index (BUI panel 3.4c), which incorporates subindices reflecting dry conditions on longer time scales, was also above the 1990-2020 maximum for the whole of June; both the Duff

moisture code (DMC, 3.4e), which reflects fuel-bed moisture on weekly time scales, and the drought code (DC, panel 3.4f), which reflects months-long drought conditions, exceeded anything observed in June between 1990-2020 and reached levels more typically experienced in August, at the peak of the fire season. Although the DSR strongly correlates to highs in the ISI, the extreme fire-weather conditions seen over the Pantanal occurred due to the co-occurrence of extreme seasonal values in fuel-bed drying across long-term (DC and DMC) and short-term (FFMC and wind) effects. This reflects the importance of the extremely low rainfall observed since mid-April (Figure 3.5a) and the long-maintained highs in rapid drying effects (Figure 3.4d).

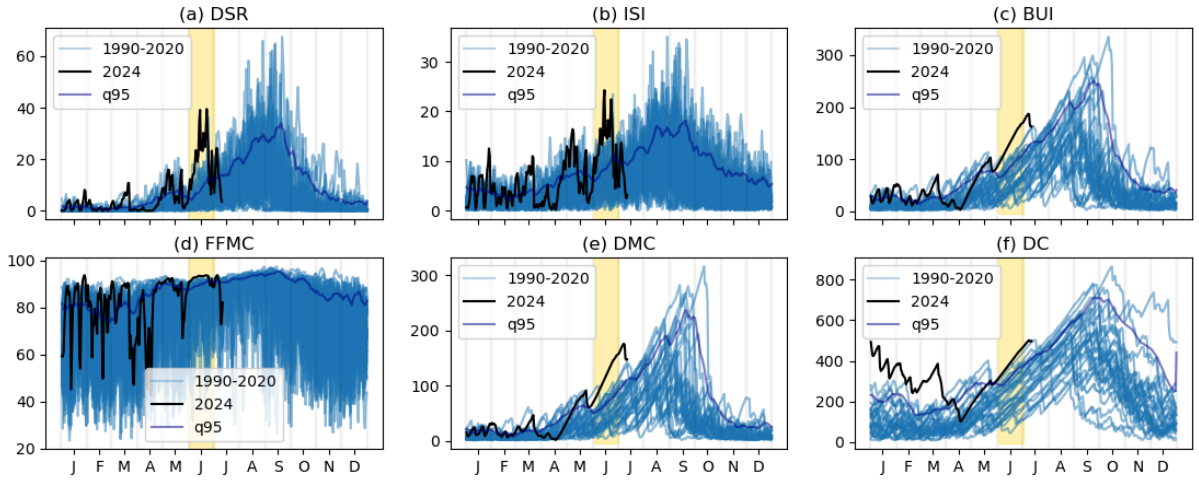

Figure 3.4: *Distribution of DSR and sub-indices averaged over the Brazilian Pantanal (ERA5). Blue lines indicate daily values from 1990-2020; black line indicates 2024 values. June is highlighted in yellow.*

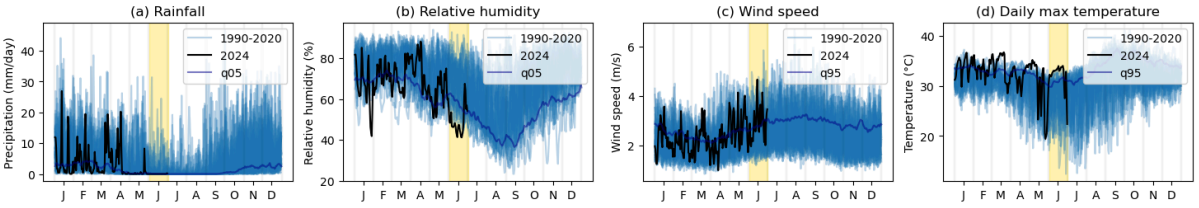

Figure 3.5: *Distribution of key weather variables averaged over the Brazilian Pantanal (ERA5). Blue lines indicate daily values from 1990-2020; black line indicates 2024 values; dark blue line is the 95th percentile of the 15-day smoothed climatology (lower percentile for rainfall and relative humidity, upper percentile for temperature and wind speed). June is highlighted in yellow.*

Figure 3.6 shows annual time series of the June mean of key weather variables used in the computation of the DSR, averaged over the study region. June 2024 was unusually hot, dry and windy even in the current climate, with the lowest June precipitation and relative humidity, and highest mean daily maximum temperatures and wind speed, recorded in the past 50 years; for all four of the key variables to be extreme simultaneously in this way remains unusual. Identifying which of these factors has contributed most to the increased DSR is beyond the scope of this report, but there is evidence of a decline in precipitation in recent decades, while relative humidity has also decreased as temperatures increase. Many past studies have robustly linked rising temperatures to human activity, so this trend is likely to continue; changes in rainfall in the region are discussed in more detail in Section 3.2.

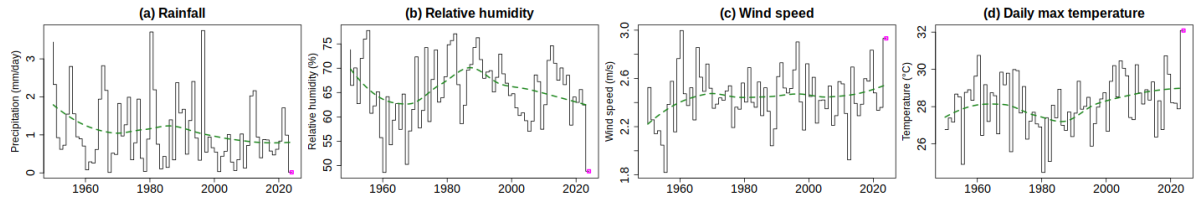

Figure 3.6: *Time series of June mean of key weather variables averaged over the Brazilian Pantanal (ERA5). In each panel the pink dot marks June 2024, and the dashed green line is a nonparametric Loess smoother.*

3.2 Annual precipitation

Figure 3.7 shows the time series of annual precipitation in the Brazilian Pantanal in the ERA5, MSWX and CHIRPS datasets. We note that the MERGE dataset only has 24 years of data available; for an extreme value distribution, this would not be long enough to produce reliable estimates of the parameters of the statistical model, but for the normal distribution used here, the mean trend at least is likely to be well estimated, albeit with high uncertainty; furthermore, the fitted model results are compatible with the results from the other datasets, suggesting that this shorter time series is representative of the longer-term trends. We therefore retain the MERGE dataset alongside the longer time series in the final attribution analysis. The datasets are highly correlated after 2001 (all Pearson correlation coefficients > 0.7), but diverge prior to this, wth ERA5 and MSWX somewhat wetter than CHIRPS from 1980-2000. In all datasets the linear trend determined by GMST is close to the nonparametrically smoothed trend (dashed green line), although four out of the last five years experienced much lower rainfall than expected even in the current climate (see also Figure 1.4a); it is not clear whether this is the result of natural variability or related to some other factor that is not included in the statistical model. As part of the exploratory analysis, an extended version of the model was fitted, including the detrended Niño3.4 index as an additional covariate; however, this did not result in an improved model fit, so we focus here only on the relationship between rainfall and GMST.

In all of the datasets, 2023-24 was the driest year on record; however, the estimated return periods for this event are very variable, with the best estimates ranging between 40 years in ERA5 and 226 years in MSWX (Table 3.2). This is largely due to the difficulty of estimating the return period of such an extreme event from a relatively short time series; for MERGE, in particular, the return period estimate is very unstable. For the attribution analysis, we treat this as a 1-in-100-year event, reflecting the consensus of the four datasets.

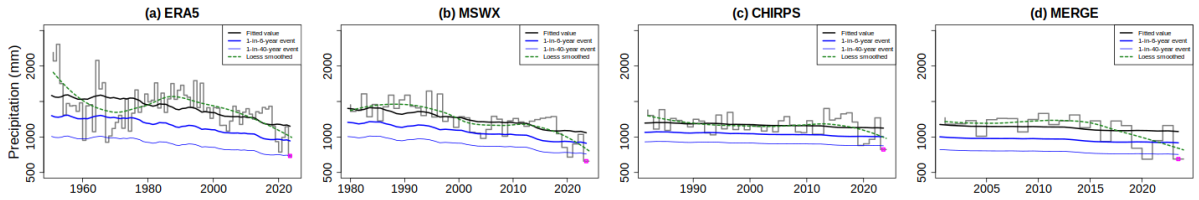

Figure 3.7: *Time series of annual precipitation averaged over the study region in four gridded observational datasets: ERA5, MSWX, CHIRPS and MERGE. The heavy black line indicates the mean of the nonstationary distribution, with the 6-year and 40-year effective return levels in each year in blue. The dashed green line is a nonparametric Loess smoother; the pink dot marks the 2024 total.*

Table 3.2: *Estimated return period of July 2023-June 2024 accumulated precipitation, relative change in annual, and change in likelihood of exceeding the observed 2023-24 accumulated precipitation between the 2024 climate and a 1.2ºC cooler climate, in the three observational datasets used in the study.*

	ERA5	MSWX	CHIRPS	MERGE
Return period	39.7	226	115	107
% change in DSR	-29.6 (-37.8, -13.6)	-34.2 (-53.5, -21.8)	-9.34 (-22.2, 5.6)	-18.3 (-34.6, -13)
Probability ratio	17.0 (3.88, 73.8)	207 (34.7, 582252)	6.11 (0.27, 167)	10.2 (5.63, 13841)

The fitted trend in annual precipitation in each observational dataset is shown as a function of GMST in Figure 3.8. All datasets show a reduction in annual rainfall in this region, of between 9% and 34% compared to the expected rainfall in the preindustrial climate (Table 3.2); this trend is statistically significant in all of the datasets except CHIRPS, which is somewhat drier than ERA5 and MSWX from 1980-2000.

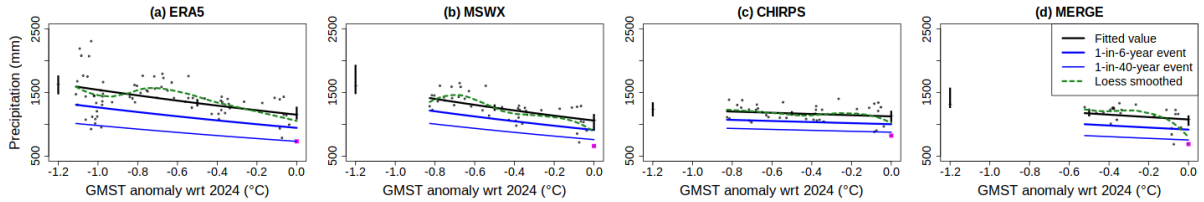

Figure 3.8: *Linear trend in annual precipitation in ERA5, MSWX, CHIRPS and MERGE as a function of GMST. The thick black line denotes the mean of the fitted distribution, and the blue lines show estimated 6- and 40-year return levels. The dashed green line is a nonparametric Loess smoother. The vertical lines show the 95% confidence interval for the mean of the distribution in the 2024 climate, a 0.5ºC cooler 2000 climate and a hypothetical 1.2ºC cooler climate. The 2024 observation is highlighted in magenta.*

Figure 3.9 shows the expected change in return levels of the 2023-24 rainfall associated with a 1.2°C change in GMST. In general the observations (points) lie close to the line indicating the expected values; however, the very lowest points - corresponding to the very dry years in 2020, 2021 and 2024 - lie well below the expected, and in some cases outside of the shaded area representing a 95% confidence interval. This suggests that the return period of the 2023-2024 drought in the current climate is actually lower than estimated by the statistical model; only in ERA5, does the model fit the lower tail of the distribution well, and there the return period was estimated to be just 40 years. As a result the estimated probability ratios are again very uncertain, with best estimates that the event is 6-207 times more likely (Table 3.2).

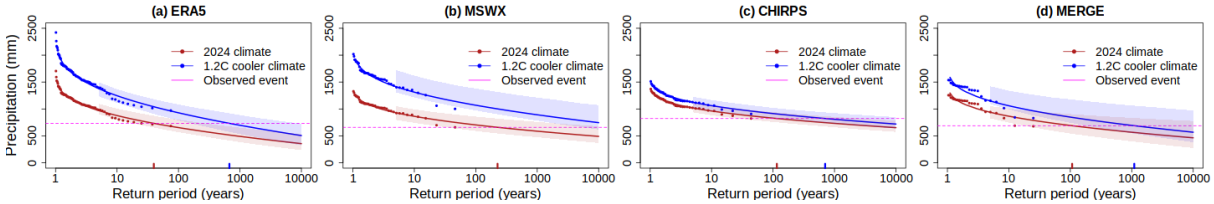

Figure 3.9: *Return levels for annual precipitation over the Brazilian Pantanal at the 2024 GMST (red lines) and 1.2°C lower GMST (blue line), estimated from the statistical model. Shaded regions represent 95% confidence intervals obtained via a bootstrapping procedure. The pink line shows the precipitation during 2023-24. Red and blue ticks at the x axis indicate the estimated return level of June 2024 in the 2024 climate and 1.2°C cooler climate respectively.*

4 Model evaluation

The climate models are first evaluated against the gridded observational data products for their ability to capture the seasonal and spatial patterns of daily maximum temperatures and precipitation in the study region. The models are then evaluated on how closely the parameters of the fitted statistical model (in this case, the standard deviation of the normal distribution for both logDSR and annual precipitation) match those estimated using the observational datasets. The models are labelled as 'good' if the best estimate of each parameter falls within the bounds estimated from the observations; 'reasonable' if the confidence interval for the model overlaps with the range estimated from the observations; or 'bad' if the ranges do not overlap. If the model is 'good' for all criteria, we give it an overall rating of 'good'. We rate the model as 'reasonable' or 'bad', if it is rated 'reasonable' or 'bad', respectively, for at least one criterion. In Tables 4.1 and 4.2 below we show the results of the model validation for logDSR and annual precipitation over the Brazilian Pantanal. In each case, if more than five models achieve a 'good' evaluation overall, then only these models are included in the attribution; if five models or fewer achieve this, then models deemed 'reasonable' are also included. In all cases, models deemed 'good' or 'reasonable' were included in the final analysis. Most of the models were able to capture the timing of the seasonal cycle of precipitation, but not the amplitude or length of the rainy season; many also failed to correctly replicate the shape of the temperature distribution. Plots comparing the seasonal cycle for each model can be found in Figures A2.1-A2.2 (for precipitation) and A2.3-A2.4 (for daily maximum temperatures).

Table 4.1: *Evaluation of the climate models considered for attribution of June logDSR over the Brazilian Pantanal. For each model, the best estimate of the scale parameter is shown, along with a 95% confidence obtained via bootstrapping. The overall evaluation is shown in the right-hand column. There is very little spatial variation in precipitation or temperature over the study region and all models were judged 'reasonable' in this respect, so the results of the spatial evaluation are not shown.*

	Model / Observations	Seasonal cycle (pr)	Seasonal cycle (tmax)	Sigma	Overall conclusion
Obs	ERA5			0.816 (0.690 ... 0.921)	
	MERRA2			0.703 (0.530 ... 0.822)	
	MSWX			0.761 (0.631 ... 0.849)	
CMIP6	CanESM5	good	bad	0.679 (0.578 ... 0.741)	bad
	CMCC-ESM2	good	bad	0.357 (0.269 ... 0.423)	bad
	EC-Earth3	good	reasonable	0.987 (0.677 ... 1.24)	bad
	INM-CM4-8	good	bad	0.806 (0.570 ... 0.964)	bad
	INM-CM5-0	good	bad	0.669 (0.497 ... 0.812)	bad
	IPSL-CM6A-LR	good	bad	0.441 (0.338 ... 0.512)	bad
	MIROC6	good	reasonable	0.426 (0.337 ... 0.488)	reasonable
	MPI-ESM1-2-HR	reasonable	reasonable	0.800 (0.579 ... 0.974)	reasonable
	MPI-ESM1-2-LR	reasonable	reasonable	0.709 (0.559 ... 0.819)	reasonable
	MRI-ESM2-0	good	reasonable	0.290 (0.216 ... 0.340)	reasonable

	NorESM2-MM	good	good	0.365 (0.255 ... 0.458)	reasonable
CORDEX SAM-22	MOHC-HadGEM2-ES RegCM4-7	good	reasonable	0.677 (0.504 ... 0.797)	reasonable
	MOHC-HadGEM2-ES REMO2015	good	good	0.622 (0.487 ... 0.721)	good
	MPI-M-MPI-ESM-LR REMO2015	good	good	0.502 (0.381 ... 0.584)	bad
	MPI-M-MPI-ESM-MR RegCM4-7	good	bad	0.433 (0.347 ... 0.495)	bad
	NCC-NorESM1-M RegCM4-7	good	bad	0.340 (0.197 ... 0.481)	bad
	NCC-NorESM1-M REMO2015	reasonable	bad	0.436 (0.320 ... 0.523)	bad
CORDEX SAM-44	CCCma-CanESM2 RCA4	reasonable	reasonable	0.485 (0.340 ... 0.598)	bad
	CCCma-CanESM2 WRF341I	reasonable	reasonable	0.750 (0.565 ... 0.891)	reasonable
	CNRM-CERFACS-CNRM-CM5 RCA4	reasonable	reasonable	0.757 (0.630 ... 0.839)	reasonable
	QCCCE-CSIRO-Mk3-6-0 RCA4	good	bad	0.606 (0.482 ... 0.697)	bad
	ICHEC-EC-EARTH RCA4	reasonable	reasonable	0.399 (0.313 ... 0.466)	reasonable
	IPSL-IPSL-CM5A-MR RCA4	reasonable	bad	0.305 (0.213 ... 0.364)	bad
	MIROC-MIROC5 RCA4	reasonable	bad	0.381 (0.287 ... 0.448)	bad
	MOHC-HadGEM2-ES RCA4	reasonable	good	0.793 (0.583 ... 0.939)	reasonable
	MPI-M-MPI-ESM-LR RCA4	reasonable	reasonable	0.412 (0.318 ... 0.478)	reasonable
	NCC-NorESM1-M RCA4	reasonable	reasonable	0.319 (0.224 ... 0.390)	reasonable
	NOAA-GFDL-GFDL-ESM2M RCA4	reasonable	reasonable	0.614 (0.482 ... 0.707)	reasonable

Table 4.2: *Evaluation of the climate models considered for attribution of annual rainfall over the Brazilian Pantanal. For each model, the best estimate of the scale parameter is shown, along with a 95% confidence obtained via bootstrapping. The overall evaluation is shown in the right-hand column. There is very little spatial variation in precipitation or temperature over the study region and all models were judged 'reasonable' in this respect, so the results of the spatial evaluation are not shown.*

	Model / Observations	**Seasonal cycle (pr)**	**Sigma**	**Overall conclusion**
Obs	ERA5-1979		0.142 (0.104 ... 0.165)	
	MSWX		0.144 (0.105 ... 0.167)	
	CHIRPS		0.113 (0.088 ... 0.131)	
CMIP6	CanESM5	good	0.169 (0.113 ... 0.213)	bad

	CMCC-ESM2	good	0.098 (0.078 ... 0.113)	good
	EC-Earth3	good	0.135 (0.108 ... 0.156)	good
	INM-CM4-8	good	0.113 (0.089 ... 0.129)	good
	INM-CM5-0	good	0.126 (0.099 ... 0.145)	good
	IPSL-CM6A-LR	good	0.063 (0.05 ... 0.073)	reasonable
	MIROC6	good	0.159 (0.128 ... 0.182)	good
	MPI-ESM1-2-HR	reasonable	0.091 (0.069 ... 0.107)	reasonable
	MPI-ESM1-2-LR	reasonable	0.106 (0.084 ... 0.121)	reasonable
	MRI-ESM2-0	good	0.123 (0.095 ... 0.145)	good
	NorESM2-MM	good	0.152 (0.12 ... 0.177)	good
CORDEX SAM-22	MOHC-HadGEM2-ES RegCM4-7	good	0.146 (0.114 ... 0.169)	good
	MOHC-HadGEM2-ES REMO2015	good	0.119 (0.092 ... 0.137)	good
	MPI-M-MPI-ESM-LR REMO2015	good	0.137 (0.107 ... 0.162)	good
	MPI-M-MPI-ESM-MR RegCM4-7	good	0.132 (0.104 ... 0.156)	good
	NCC-NorESM1-M RegCM4-7	good	0.174 (0.138 ... 0.199)	bad
	NCC-NorESM1-M REMO2015	reasonable	0.15 (0.112 ... 0.18)	reasonable
CORDEX SAM-44	CCCma-CanESM2 RCA4	reasonable	0.123 (0.096 ... 0.143)	reasonable
	CCCma-CanESM2 WRF341I	reasonable	0.142 (0.113 ... 0.164)	reasonable
	CNRM-CERFACS-CNRM-CM5 RCA4	reasonable	0.11 (0.082 ... 0.131)	reasonable
	QCCCE-CSIRO-Mk3-6-0 RCA4	good	0.156 (0.119 ... 0.182)	good
	ICHEC-EC-EARTH RCA4	reasonable	0.139 (0.108 ... 0.162)	reasonable
	IPSL-IPSL-CM5A-MR RCA4	reasonable	0.143 (0.115 ... 0.161)	reasonable
	MIROC-MIROC5 RCA4	reasonable	0.105 (0.083 ... 0.12)	reasonable
	MOHC-HadGEM2-ES RCA4	reasonable	0.1 (0.079 ... 0.113)	reasonable
	MPI-M-MPI-ESM-LR RCA4	reasonable	0.094 (0.067 ... 0.119)	reasonable
	NCC-NorESM1-M RCA4	reasonable	0.109 (0.083 ... 0.128)	reasonable
	NOAA-GFDL-GFDL-ESM2M RCA4	reasonable	0.14 (0.098 ... 0.177)	reasonable

5 Multi-method multi-model attribution

Tables 5.1 and 5.2 show probability ratios (PR) and changes in intensity (ΔI) in June logDSR and annual precipitation, for the observational data products and for and for those models that passed the evaluation described in Section 4. These changes are synthesised into a single overarching attribution result in Section 6.

Table 5.1: *Event magnitude, probability ratio and change in intensity for 35-year June logDSR over the Brazilian Pantanal for observational datasets and each model that passed evaluation: (a) from the preindustrial climate to the present and (b) from the present to 2°C above preindustrial.*

		(a) -1.2C vs present		(b) Present vs +0.8C	
Model / Observations	**35-year event (logDSR)**	**Probability ratio**	**Change in intensity (˚C)**	**Probability ratio**	**Change in intensity (˚C)**
ERA5	6.4	4.7 (0.67 ... 32)	65 (-11 ... 203)		
MERRA2	7.3	121 (3.6 ... 20660)	207 (33 ... 637)		
MSWX	5.6	699 (11 ... 498506)	366 (69 ... 1309)		
MIROC6	6.8	2.0 (0.51 ... 10)	16 (-14 ... 59)	1.5 (0.88 ... 2.4)	9.3 (-3.0 ... 20)
MPI-ESM1-2-HR	4.8	2.2 (0.66 ... 9.0)	29 (-13 ... 88)	1.9 (1.3 ... 2.7)	20 (7.8 ... 30)
MPI-ESM1-2-LR	4.4	10 (2.9 ... 49)	122 (46 ... 234)	2.7 (2.0 ... 3.8)	35 (25 ... 46)
MRI-ESM2-0	5.6	122 (20 ... 2505)	85 (51 ... 143)	2.7 (2.0 ... 3.8)	17 (12 ... 23)
NorESM2-MM	6.6	7.6 (1.2 ... 58)	38 (2.7 ... 77)	3.5 (2.4 ... 5.1)	23 (16 ... 29)
SAM-22 MOHC-HadGEM2-ES RegCM4-7	7.3	4.8 (0.93 ... 33)	49 (-1.7 ... 127)	1.8 (1.2 ... 2.9)	16 (3.5 ... 27)
SAM-22 MOHC-HadGEM2-ES REMO2015	5.4	6.3 (1.1 ... 79)	53 (1.7 ... 138)	1.9 (1.2 ... 2.9)	16 (4.6 ... 27)
SAM-44 CCCma-CanESM2 WRF341I	5.4	1.3 (0.43 ... 4.0)	8.6 (-24 ... 51)	1.1 (0.76 ... 1.6)	3.6 (-8.1 ... 15)
SAM-44 CNRM-CERFACS-CNRM-CM5 RCA4	6.5	3.9 (0.58 ... 50)	47 (-16 ... 157)	1.6 (0.93 ... 2.9)	15 (-2.4 ... 29)
SAM-44 ICHEC-EC-EARTH RCA4	6.3	2.8 (0.64 ... 17)	20 (-9.1 ... 58)	1.5 (0.88 ... 2.6)	7.8 (-2.6 ... 19)
SAM-44 MOHC-HadGEM2-ES RCA4	5.9	3.2 (0.79 ... 19)	40 (-7.5 ... 105)	2.3 (1.7 ... 3.3)	24 (15 ... 33)
SAM-44 MPI-M-MPI-ESM-LR RCA4	6.3	7.1 (1.6 ... 63)	38 (8.4 ... 76)	2.3 (1.3 ... 3.9)	17 (5.7 ... 25)

SAM-44 NCC-NorESM1-M RCA4	6.6	2.9 (0.43 ... 27)	17 (-13 ... 56)	1.7 (0.86 ... 3.0)	8.0 (-2.4 ... 17)
SAM-44 NOAA-GFDL-GFDL-ESM2M RCA4	5.9	1.5 (0.27 ... 22)	12 (-32 ... 89)	2.2 (1.3 ... 3.7)	19 (5.8 ... 29)

Table 5.2: *Event magnitude, probability ratio and change in intensity for 100-year annual rainfall over the Brazilian Pantanal for observational datasets and each model that passed evaluation: (a) from the preindustrial climate to the present and (b) from the present to 2°C above preindustrial.*

		(a) -1.2C vs present		(b) Present vs +0.8C	
Model / Observations	**35-year event (logDSR)**	**Probability ratio**	**Change in intensity (˚C)**	**Probability ratio**	**Change in intensity (˚C)**
ERA5-1979	788	168 (34 ... 215219)	-32 (-51 ... -20)		
MSWX	704	208 (36 ... 357975)	-34 (-53 ... -22)		
CHIRPS	830	6 (0.3 ... 169)	-9 (-22 ... 6.4)		
CMCC-ESM2	950	0.7 (0.3 ... 1.9)	1.8 (-2.9 ... 6.6)	0.4 (0.3 ... 0.6)	3.8 (2.2 ... 5.2)
EC-Earth3	1037	1.9 (0.9 ... 4.6)	-3.7 (-8.8 ... 0.5)	1.1 (0.9 ... 1.5)	-0.6 (-2.5 ... 0.7)
INM-CM4-8	892	0.1 (0.1 ... 0.3)	13 (6.6 ... 20)	0.5 (0.3 ... 0.8)	3.5 (1.3 ... 5.5)
INM-CM5-0	890	0.2 (0.1 ... 0.8)	10 (1.1 ... 17)	1 (0.6 ... 1.5)	0 (-2.9 ... 2.9)
MIROC6	855	2.1 (0.6 ... 10)	-5.3 (-14 ... 4.3)	1.4 (0.9 ... 2.3)	-2.4 (-6.1 ... 0.5)
MRI-ESM2-0	996	7.4 (2.6 ... 23)	-11 (-16 ... -5.6)	1.6 (1.2 ... 2.3)	-3.1 (-5.7 ... -1)
NorESM2-MM	836	1 (0.4 ... 2.7)	0 (-8.6 ... 10)	1.7 (1.2 ... 2.6)	-5.4 (-9 ... -1.9)
SAM-22 MOHC-HadGEM2-ES RegCM4-7	721	2.3 (0.8 ... 8.6)	-6.4 (-14 ... 1.8)	1.1 (0.8 ... 1.7)	-1 (-5.6 ... 2.6)
SAM-22 MOHC-HadGEM2-ES REMO2015	1158	3.2 (0.7 ... 29)	-6.2 (-13 ... 2)	1.5 (1 ... 2.3)	-2.6 (-5.9 ... 0)
SAM-22 MPI-M-MPI-ESM-LR REMO2015	1043	2.1 (0.5 ... 17)	-5.1 (-16 ... 5.3)	0.9 (0.5 ... 1.6)	0.5 (-3.4 ... 4.7)
SAM-22 MPI-M-MPI-ESM-MR RegCM4-7	833	0.7 (0.1 ... 3.1)	2.6 (-7.2 ... 16)	0.6 (0.3 ... 1.2)	3.5 (-1.3 ... 8)
SAM-44 QCCCE-CSIRO-Mk3-6-0 RCA4	826	1.7 (0.4 ... 14)	-4.9 (-21 ... 8.6)	1.2 (0.8 ... 1.9)	-1.9 (-6.3 ... 2.1)

6 Hazard synthesis

We now evaluate the evidence for the influence of anthropogenic climate change in both June DSR and July-June annual precipitation in the Brazilian Pantanal by calculating the probability ratio and

change in intensity for both observations and climate models. Models which do not pass the validation tests described in Section 4 are excluded from the analysis. The aim is to synthesise results from models that pass the evaluation along with the observation-based products, to give an overarching attribution statement for each index. Figures 6.1-6.4 show the changes in probability and relative intensity of the event of interest in both the observations (blue) and climate models (red). The best estimate for each dataset is marked with a black triangle. A term to account for intermodel spread is added in quadrature to the natural variability of the models: this is shown in the figures as white boxes around the light red bars. The dark red bar shows the model average, consisting of a weighted mean using the (uncorrelated) uncertainties due to natural variability plus the term representing intermodel spread (the white bars). Observation-based products and models are combined into a single result in two ways. Firstly, we neglect common model uncertainties beyond the intermodel spread already incorporated in the model average, and compute the precision-weighted average of models (dark red bar) and observations (dark blue bar): this weighted mean is indicated by the magenta bar. To account for the fact that, due to common model uncertainties, model uncertainty can be larger than the intermodel spread, we also show an unweighted direct average of observations (dark blue bar) and models (dark red bar) contributing 50% each, indicated by the white box in the synthesis figures.

Figure 6.1 shows the changes in probability and relative intensity of a 1-in-35-year event associated with an increase of 1.2 °C in GMST. As discussed in Section 3.1, all of the observational gridded products exhibit a relatively strong increase in June DSR, but with very high uncertainty; this is reflected in the width of the dark blue bar representing the overall observational result. The climate models also consistently simulate an increase in June DSR in the Brazilian Pantanal, but of somewhat lower magnitude. Because the models produce lower-variance estimates (narrower bars) with similar best estimates, the overall model result (dark red bar) is much narrower than the overall result from the observations, and is given much more weight in the overall synthesis (purple bar). The white bar indicating the unweighted mean of the overall observational and model results is much wider, and skewed by the observations to include the possibility of much larger changes in DSR due to anthropogenic warming. Given the high uncertainty in the observations and the strong agreement, we report the figures from weighted synthesis as a conservative estimate of the change in June DSR due to 1.2 °C of anthropogenic warming: a 39% increase in June DSR (95% confidence interval: 13-71% increase); and it is estimated to be 4.6 times more likely that a June DSR as high as that observed in 2024 will occur now than in a preindustrial climate (1.1 - 19.9 times more likely). After a further increase of 0.8°C (that is, with total warming of 2 °C with respect to the preindustrial climate), June DSR is projected to increase by a further 16.5% (5.3 - 28.8%), and what is currently a 1-in-35 year event is projected to become twice as likely (1.3 - 3.1 times more likely) (Figure 6.2).

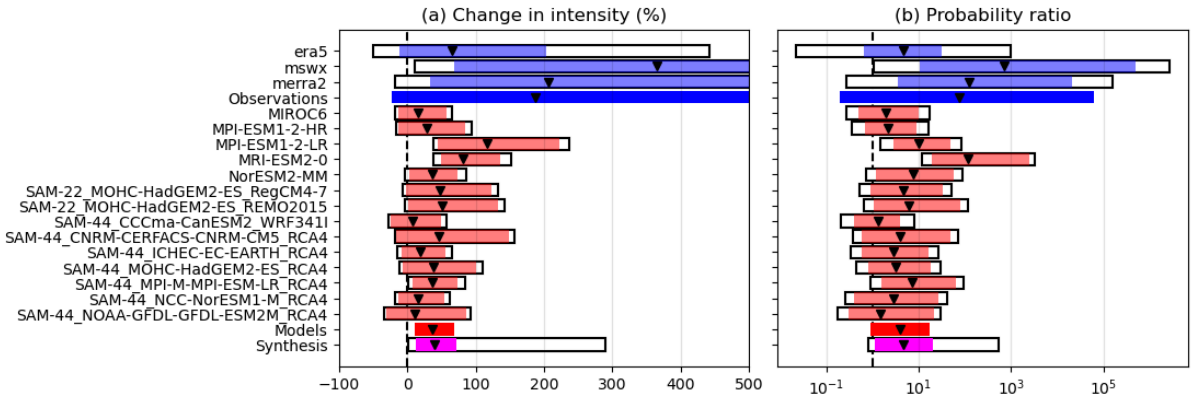

Figure 6.1: *Synthesis of (left) probability ratios and (right) relative intensity changes when comparing the return period and magnitudes of June DSR in the Brazilian Pantanal between the current climate and a 1.2C cooler climate. See text for further details. The x-axis in (a) truncated at 500 to avoid obscuring the model results: for MSWX the upper bound is 1309 (2001 including representation uncertainty); for MERRA2 the upper bound is 637 (1079 including representation uncertainty); for the observations overall, the upper bound is 993.*

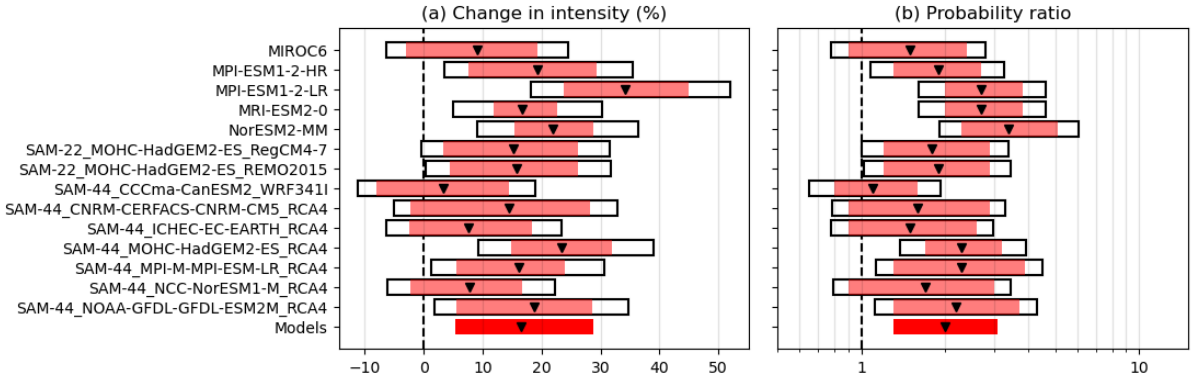

Figure 6.2: *As Figure 6.1, synthesising changes in June DSR between the current climate and a 0.8C warmer climate (that is, a climate that is 2C warmer than preindustrial). See text for further details.*

The picture is less clear for annual precipitation in the region (Figure 6.3). The individual observation-based datasets all show a drying trend, although the uncertainty is high enough that the overall observational result (dark blue bar) includes the possibility of no change (best estimate from obs: -23.5%; 95 confidence interval -46 to +5%); however, this is due to a single dataset that simulates a lower trend, so is likely to be a conservative estimate. While many of the models that passed validation exhibit a slight drying trend, this is only statistically significant in one model, and two models actually simulate a wetting in this region; however, it is known that models may not replicate historical rainfall trends in this region well (Gomes et al., 2021), due to the difficulty of simulating the MJO and SACZ (see Section 1.2). As a result, the overall result from the models (dark red bar) is that rainfall totals have not changed; this absence of a clear trend is projected to continue into the future (Figure 6.4). This discrepancy between the climate models and the observations in terms of the projected rainfall trend may, in part, explain the difference between observed and modelled trends in DSR (Figure 6.1). Because of this, we are unable to quantify the contribution of climate change to the observed drying trend, but are confident that anthropogenic activity has contributed to lower levels of rainfall in the Brazilian Pantanal, partly due to factors such as land use changes including deforestation both locally and in the Amazon and Cerrado (Bergier et al., 2018; Marques et al., 2021).

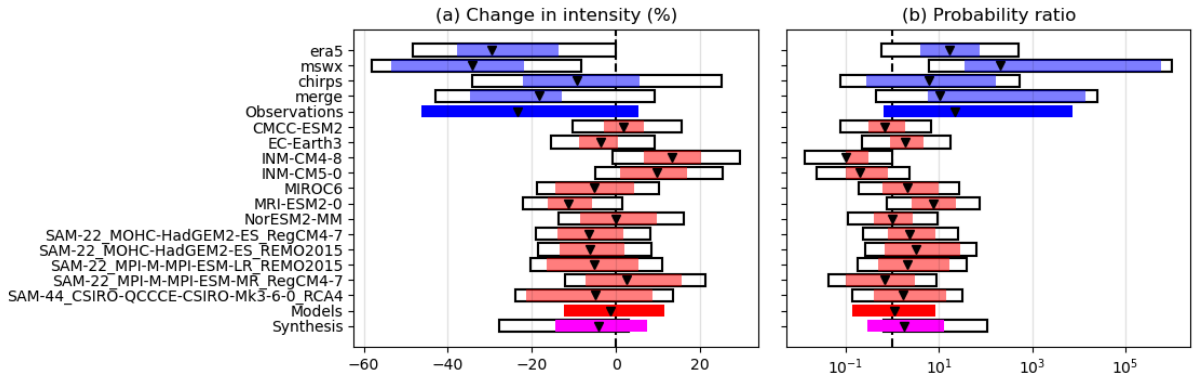

Figure 6.3: *Synthesis of (left) probability ratios and (right) relative intensity changes when comparing the return period and magnitudes of July-June annual precipitation in the Brazilian Pantanal between the current climate and a 1.2C cooler climate. See text for further details.*

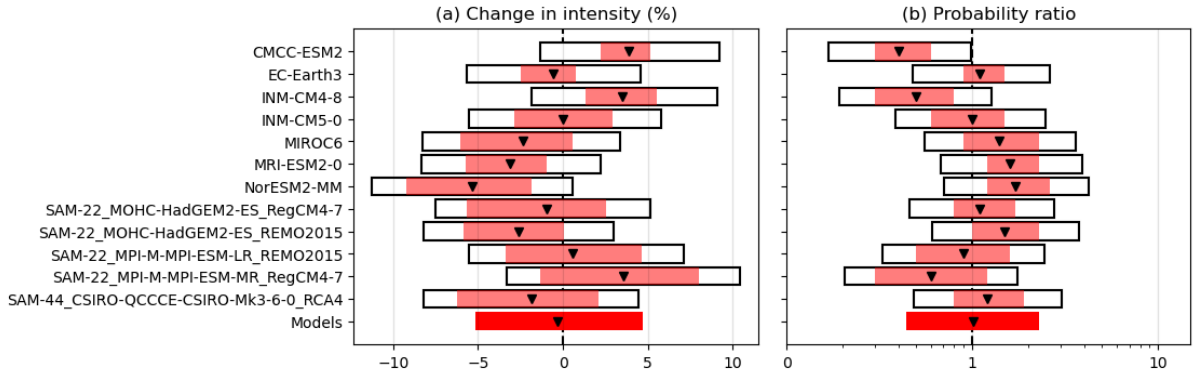

Figure 6.4: *As Figure 6.3, synthesising changes in annual precipitation between the current climate and a 0.8C warmer climate (that is, a climate that is 2C warmer than preindustrial). See text for further details.*

7 Vulnerability and exposure

The Pantanal comprises 17 million hectares of unique biodiversity with high species richness, with approximately 4,700 distinct plant and animal species, provides significant ecosystem services for the surrounding area, supports the livelihoods of numerous Indigenous and non-Indigenous people, and is a vast carbon store (Barber, 2024). It was named a UNESCO World Heritage Site in 2000 (UNESCO). The wetlands are home to numerous rare and endangered plants and animals (including jaguars, giant river otters, giant armadillos, maned wolf, capybara, caiman, hyacinth macaw, great heron) which are frequently killed during wildfires. A landscape devastated by hazards can render future survival of animals less likely as reduced availability of food and water increases competition for scarce resources (Alho et al., 2019).

The Pantanal is the largest continuous tropical freshwater seasonal wetland (Penatti et al., 2015). Half of the year it is flooded when the Paraguay River and tributaries burst their banks, and half the year it is dry (Libonati et al., 2020). The annual flood pulse patterns are linked to seasonal rainfall and drive its diverse ecology, including seasonal savannah, deciduous forests, swamps, marshes, and numerous

lakes (Britannica, 2024, Schultz et al., 2019). Climate changes and alterations in land cover and use, especially in the highlands of the Upper Paraguay River Basin, impact the hydrology of the Pantanal floodplain. Longer periods of drought increase the risk and intensity of fires (MapBiomas, 2024). It is facing significant anthropogenic pressures including land-use practices that are degrading the natural ecosystem functioning. The relationship between the plateau and the plain of the Upper Paraguay River Basin involves complex interactions that encompass illegal and authorised deforestation – often using mismanaged fires – to clear land for intensive export-driven cattle ranching and monocropping of agricultural commodities (notably, cattle feed, and to a smaller extent, soybean plantations) (EJF, n.d.; Irigaray et al., 2020). These agribusiness practices occur mainly along roads and rivers (Alho et al., 2019). Since 2019, the Pantanal has experienced a dry period, and is expected to experience severe water scarcity this year (Geirinhas et al., 2023; Libonati et al., 2024; WWF-Brazil, 2024).

Indigenous livelihoods and practices are affected as traditional lands are destroyed, cultural practices disrupted, and people displaced. Economic activities such as tourism and agriculture are also at risk as individuals lose their crops, livestock, and resources linked to their land-based economies. Moreover, their dwellings are at risk, especially in this event where 85% of the fires impacted private properties (Gov.BR, 2024). The toll of these losses on wellbeing and mental health is also significant with depression among small, vulnerable communities increasing due to a sense of hopelessness and uncertainty about how to build back (Souza, 2024).

Deforestation in other biomes (most notably the Amazon rainforest and Cerrado) also affects climate dynamics in the Pantanal (Marques et al., 2021). In addition, there is an increased demand for the construction of tourist lodges and roads, which fragment the landscape further (Alho et al., 2019). Associated waste is either buried, left as debris, or burned (Alho et al., 2019). The construction of hydropower plants along rivers and tributaries in and upstream of the Pantanal are affecting the seasonal flood pulse and hence its fragile and unique ecology (Schultz et al., 2019), rendering the area more vulnerable to the risk of wildfires.

7.1 Legislation, policy, and funding

Wildfire legislation and fire management in the Brazilian Pantanal have undergone changes since the mid-2000s. In 2009, fire management actions were initiated in the Kadiwéu Indigenous Land in the Pantanal, near the border with Paraguay, by training Indigenous fire brigades (Ribeiro & Pereira, 2024; Oliveira, 2022). These activities initially focused on combating wildfires during the dry season and implementing prevention actions (Oliveira, 2022). They were scaled up in 2014 through the introduction of the Integrated Fire Management (IFM) program, which recommended controlled burns (Ribeiro & Pereira, 2024). The IFM came under the purview of federal authorities (Silva et al., 2024). From 2019 onwards, State governments have banned controlled burning, including for agricultural purposes such as pasture renewal. However, this ban was effective in reducing the frequency of forest fires only in the first year of its implementation (Gov.Br, 2024a, Wenzel, 2024, Martins et al., 2022). Given the complexity of variables leading to fires, the ban was viewed as a far too simplistic plan by some (Wenzel, 2024).

More recently, in July 2024, Brazil's President assigned the creation of the Brazilian National Policy for Integrated Fire Management (PNMIF) to identify the rules for burning vegetation throughout the country, outline criminal penalties for arson, and create specific rules for 'protected areas' (Gov.Br.,

2024b). The PNMIF will also have a National Committee for Integrated Fire Management (CNMIF), with representation across all levels of government and civil society (Gov.Br., 2024b). Moreover, this process and policy will integrate traditional knowledge and practices on sustainable fire use and conservation (Gov.Br., 2024b).

7.2 Ignition prevention

The main ignition source in the Pantanal wetlands is human-related, while lightning is responsible for only 1% of fire events (Menezes et al., 2022). Historically, the Pantanal has evolved with natural fires, but recent decades changes in land use, driven by the expansion of cattle breeding activities, enhanced the sensitivity of the region to fire-climate extremes (Kumar et al., 2022; Ferreira Barbosa et al., 2022).

To mitigate fire risks, several actions have been implemented. These include manual removal of undergrowth, controlled burning, and vegetation reduction, which are crucial in reducing fuel loads and preventing uncontrolled wildfires (Henn da Gama Viganó et al., 2018). At the same time, long-term changes in land use have significantly influenced fire dynamics in the Pantanal. While 85% of the Pantanal retains its native vegetation, the conversion rate of natural vegetation to anthropic use has increased from 5% in 1985 to 15% in 2022, leading to greater pressure on natural areas. In thirty-eight years, 5.4 million hectares (Mha) of native vegetation have been converted to pasture and agriculture in the highlands of the Upper Paraguay River Basin (Mapbiomas, Coleção 8). These changes contribute to the region's heightened vulnerability to fires, especially during heat waves and droughts, which create favourable conditions for large burns if ignition sources are present (Silva et al., 2022, Libonati et al., 2022a, Libonati et al., 2022b).

Protected lands, while less impacted in typical years (during which the air temperature averages 24C with 1,000-1,250 mm of rainfall annually), become highly flammable during atypical years and are significantly affected by fires from surrounding regions (Ferreira Barbosa et al., 2022). Consequently, an integrated fire management program that incorporates scientific knowledge and local socio-ecological understanding is urgently needed to avert future fire crises (Damasceno-Junior et al., 2021; Garcia et al., 2021). The proximity of fires to roads and waterways further underscores the need for strategic planning in fire prevention and ensuring accessibility for fire response operations (de Magalhães Neto & Evangelista, 2022).

7.3 Detection and warning

The Brazilian Pantanal wetlands is experiencing an unprecedented fire season this year, with fire activity intensifying unusually early (Libonati et al., 2024). According to the ALARMES platform (n.d.) from the Laboratory of Satellite Application Facilities, around 143,825 ha burned in July, representing an increase of 152% compared to the historical average. The monitoring of the burned area by the ALARMES platform is performed automatically and on a daily basis, with a spatial resolution of 500m using images from the Visible Infrared Imaging Radiometer Suite (VIIRS), active fires from the same sensor (i.e., VJ114IMGTDL_NRT and VNP14IMGT), and deep learning techniques through the BA-NET (from Burned Areas Neural Network) algorithm (Pinto et al., 2020). Serving as an early-warning tool of burned area assessment, ALARMES supports environmental agencies in fire prevention and firefighting actions.

The Brazilian National Institute for Space Research (INPE) detected 2,363 fire hotspots by June 23, 2024. This represents a 2,100% increase from June 2023, and it is a record number for any June since INPE's observations began in 1998 (Malleret, 2024; Marshall, 2024). INPE utilises satellite data from NASA instruments like the Moderate Resolution Imaging Spectroradiometer (MODIS) and Visible Infrared Imaging Radiometer Suite (VIIRS) to detect active fires (Earth Observatory, 2024). These systems provide critical information about fire hotspots, enabling timely identification of fire starts.

Additionally, Brazil's National Center for Natural Disaster Monitoring and Alerts has reported on the severe drought conditions contributing to heightened fire risk (Ministry of Science, Technology, and Innovation, 2024). Monitoring drought regions close to human pathways using high-resolution climate models and remote sensing data is also vital for early detection and intervention (Higa et al., 2022).

7.4 Wildfire protection and response

The 2024 Pantanal fires have highlighted the urgent need for effective wildfire protection and response strategies, particularly in containment and suppression efforts. These extreme fires have necessitated a range of protective measures, including evacuations, rescues, and other response activities. For instance, Escola Jatobazinho, a remote riverside school in the state of Mato Grosso do Sul, had to evacuate students due to the encroaching flames, disrupting the end of the school year (Marshall, 2024; Malleret, 2024). Such evacuations underscore the immediate threats posed by these fires and the significant challenges of ensuring safety in remote regions.

Response activities have been multifaceted and involve several organisations. In June 2024, a team of multiple ministries came together to combat the fires in the Pantanal. This team was led by the Ministry of Environment and Climate Change, with the support of other ministries, such as the Ministry of Defense that provided effective logistical support, and the Ministry of Justice and Public Security that provided physical and human resources and pursued criminal charges against individuals who may have caused fires (Gov.BR, 2024a). This year the government approved a provision measure (Measure 1241/2024), allocating an additional USD 25.2 million emergency funds to the above-mentioned ministries to combat both the Pantanal fires and the biome's water shortage (Gov.BR, 2024b).

In previous years, World Wide Fund for Nature (WWF Brasil) has provided critical logistical support, such as aircraft and vehicles, to ensure access to affected areas (WWF, 2020a). The "Respostas Emergenciais em Campo" project by WWF Brasil (2020b) focuses on prevention, firefighting, humanitarian aid, fauna protection, and research. This initiative includes equipping and training community firefighting brigades in collaboration with NGOs such as Ecoa and federal structures such as Prevfogo. It also includes distributing basic food supplies with ICV and supporting animal rescue centres (WWF, 2020). Such efforts highlight the importance of multi-agency collaborations, strategic planning, and community involvement in wildfire protection.

Despite such coordinated efforts, the containment and suppression of the Pantanal fires remain challenging. The state of Mato Grosso do Sul has established thirteen new bases to accelerate the deployment of firefighters to remote areas (Malleret, 2024). Additionally, sixty-six community and private brigades are now better prepared and integrated with government forces. However, a 24% budget cut to IBAMA, the Brazilian federal environmental protection agency, has raised concerns

about the adequacy and sustainability of the government response (INPE, 2024). Local civil society organisations have called for international aid, emphasising the need for enhanced support to prevent another disaster akin to the 2020 fires (Malleret, 2024).

Persistent hot and dry weather further complicates containment actions (Libonati et al., 2024). The Pantanal region experienced the worst June for fire activity in its recorded history, following the worst November in the previous year. This trend indicates worsening conditions as the current fire seasons progresses, raising concerns about the effectiveness of preparations and responses (Malleret, 2024). In the past, multi-agency partnerships and social connections have helped mitigate impacts on vulnerable groups, including on Indigenous communities and rural populations (WWF, 2020), and these efforts and partnerships have to be sustained

V&E conclusions

Exploring the Brazilian Pantanal fires with a focus on vulnerability and exposure is integral to better understanding the impact of a hotter and drier climate in this region. The analysis reveals the biome's susceptibility to wildfire risk and the potential for damage to local communities, biodiversity, and ecosystems. There are also impacts on the livelihoods and health of individuals living in the region who may face respiratory issues and have to cope with the challenges of rebuilding after fires.

While significant steps have been taken to address the Pantanal wildfires, there are substantial challenges to containment and suppression efforts. The current fire situation, in combination with the results of this study indicating a hotter and drier climate fueled in part by climate change, underscores the need for robust, coordinated, and well-funded firefighting strategies to mitigate the impact of future wildfires and ensure the protection of vulnerable populations, wildlife, and ecosystems.

The Brazilian National Policy for Integrated Fire Management (PNMIF) is a positive sign, signalling a new iteration of fire management which learns from previous versions, enforces fire rules and guidelines more strictly, and plans to holistically integrate Indigenous knowledge and practices within its practices. Promoting sustainable agricultural practice and reducing deforestation in surrounding ecosystems, such as the Amazon and Cerrado, can help to maintain rainfall patterns and reduce the drying trend. Moreover, developing infrastructure that is resilient to fire risks, including firebreaks and safe zones, can protect human lives and structures. By enhancing the Pantanal's resilience to climate change, it is possible to safeguard both human and ecological systems from the increasing threat of wildfires.

Data availability

Time series used in the analysis are available via the Climate Explorer.

References

All references are given as hyperlinks in the text.

Appendix

1 Additional plots for observational analysis

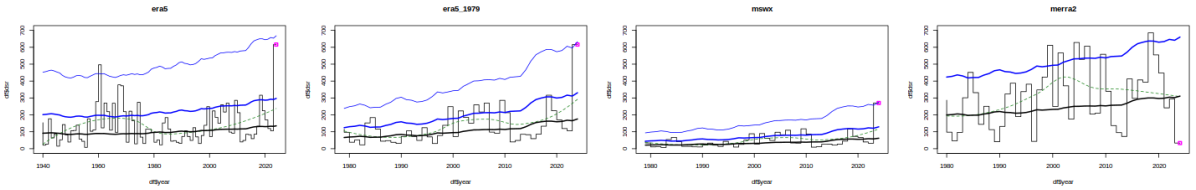

Figure A1.1: *Time series of June DSR averaged over the study region in three observational datasets: ERA5, MSWX and MERRA2. The heavy black line indicates the mean of the nonstationary distribution fitted to the full time series, with the 6-year and 40-year effective return levels in each year in blue. The dashed green line is a nonparametric Loess smoother; the pink dot marks the 2024 total. At the time of writing, data for June 2024 were not yet available for MERRA2 so the event is not shown.*

2 Model evaluation plots: seasonal cycle

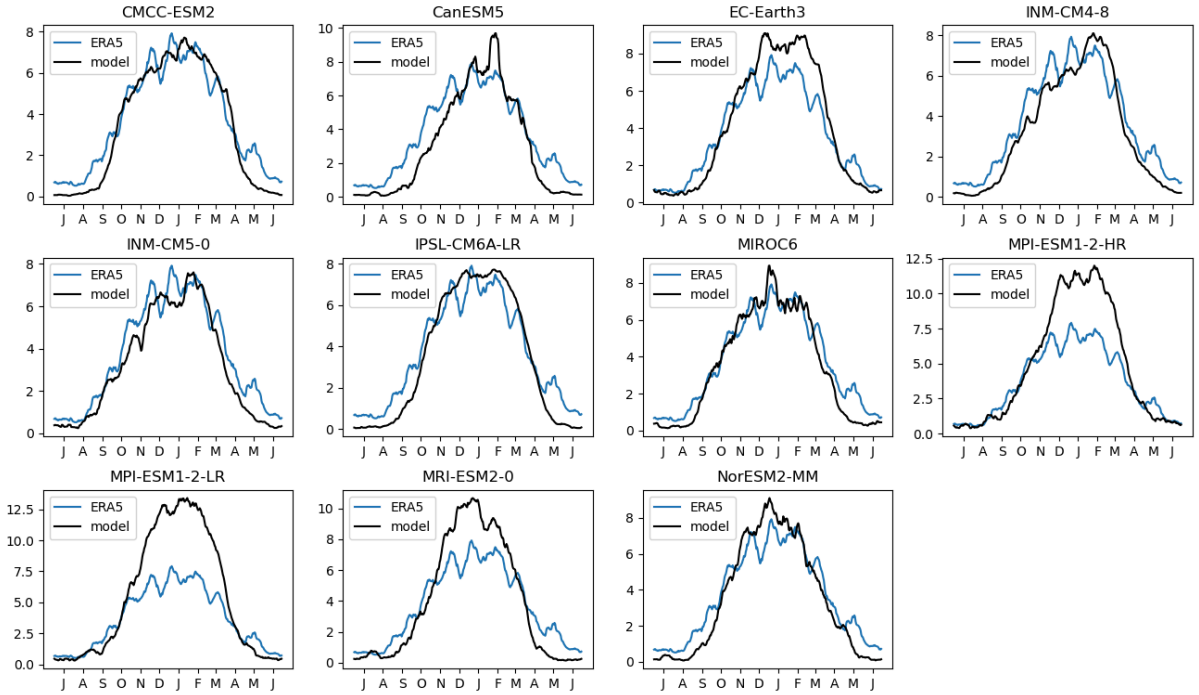

Figure A2.1: *Seasonal cycle of 15-day smoothed precipitation in CMIP6 climate models (black lines), overlaid with ERA5 (blue lines) for reference*

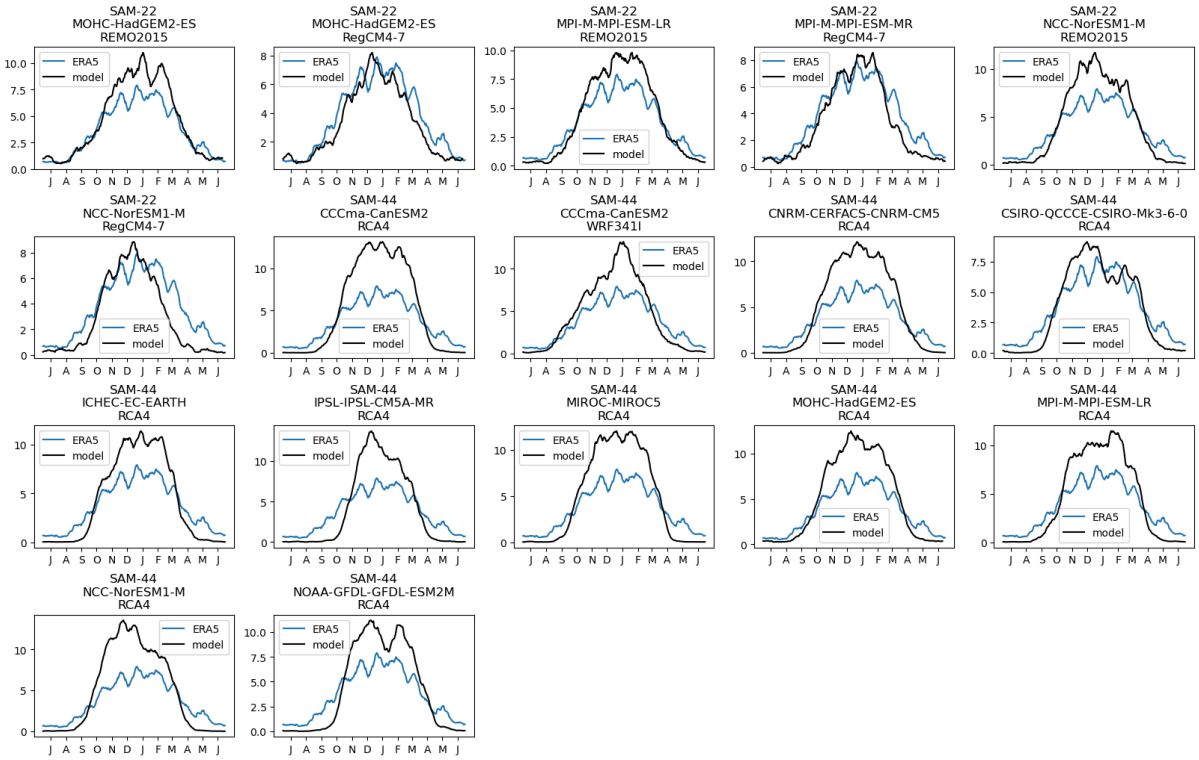

Figure A2.2: *Seasonal cycle of 15-day smoothed precipitation in CORDEX climate models (black lines), overlaid with ERA5 (blue lines) for reference*

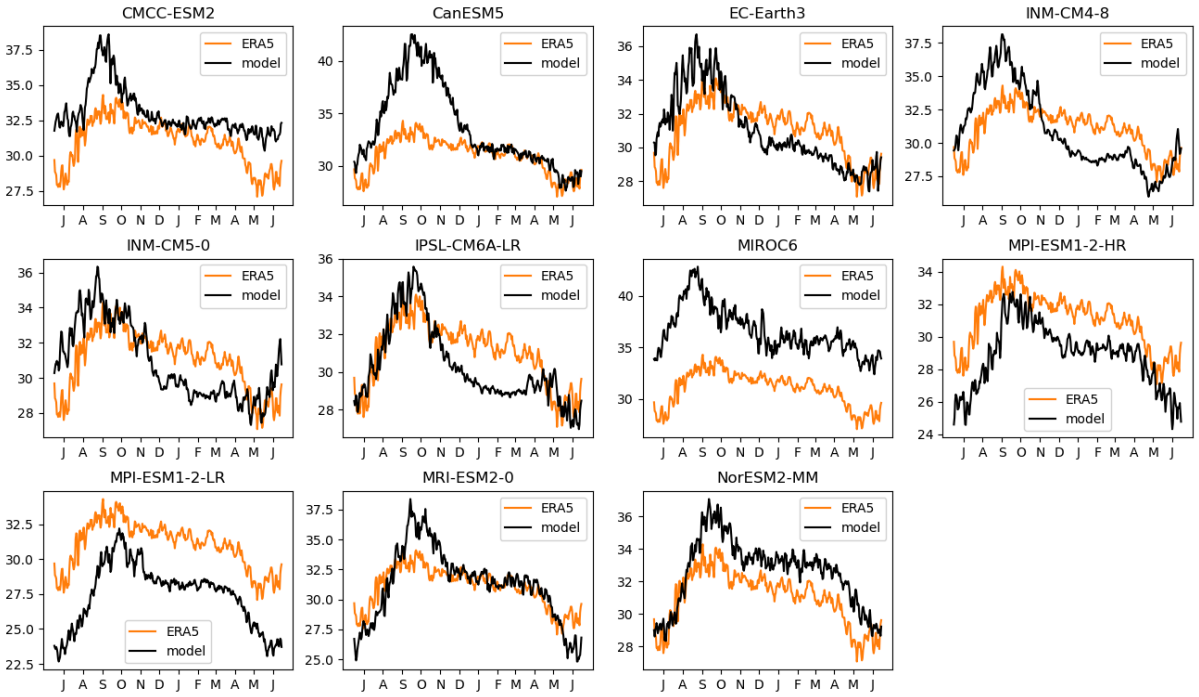

Figure A2.3: *Seasonal cycle of daily maximum temperatures in CMIP6 climate models (black lines), overlaid with ERA5 (orange lines) for reference*

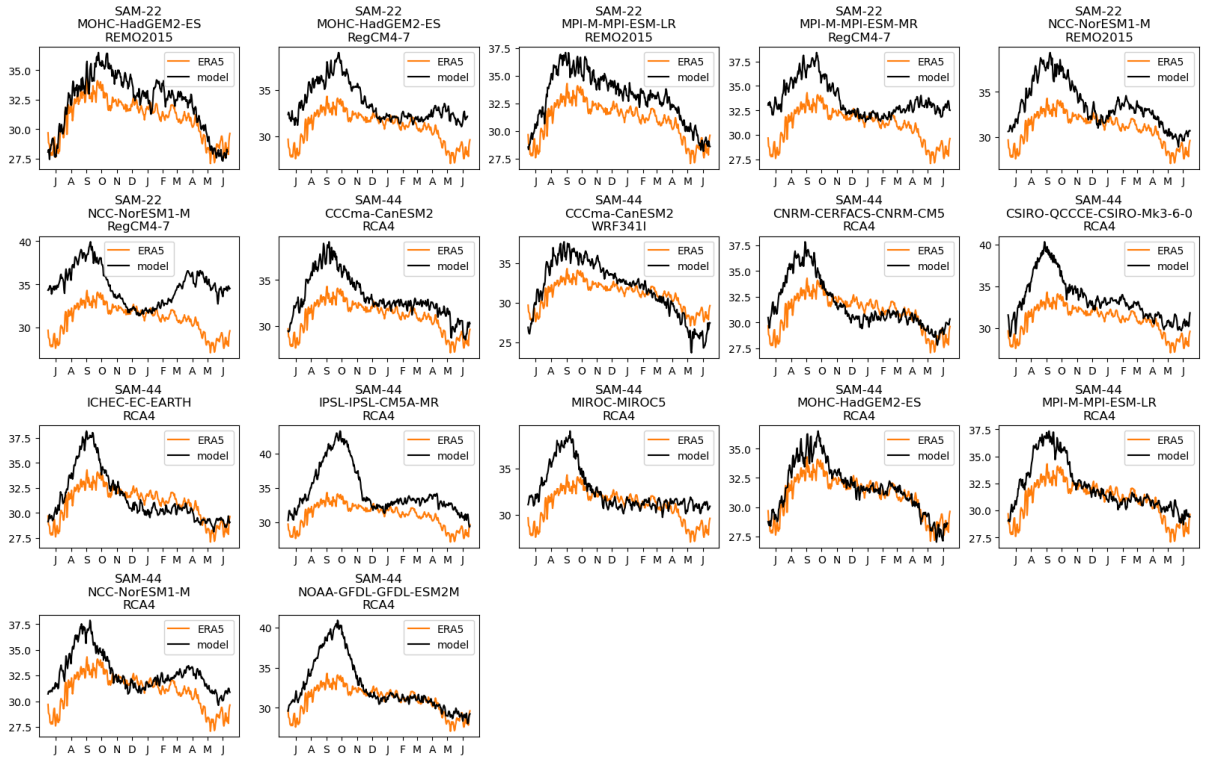

Figure A2.4: *Seasonal cycle of daily maximum temperatures in CORDEX climate models (black lines), overlaid with ERA5 (orange lines) for reference*